Lattice dynamics of zinc: Phonon structure factors*

N. J. Chesser[†‡]
Physics Department, State University of New York at Stony Brook, Stony Brook, New York 11790
Brookhaven National Laboratory, Upton, New York 11973

J. D. Axe
Brookhaven National Laboratory, Upton, New York 11973
(Received 17 September 1973)

Determination of the inelastic structure factors has been carried out for the [010] longitudinal-phonon modes of zinc. From this information the phase of the dynamical matrix element relating forces between atomic sublattices can be abstracted. Together with the measured frequencies, this gives a complete estimate of the longitudinal part of the dynamical matrix for the [010] propagation direction. Comparison with various models reveals that while the phase determined by a pseudopotential calculation shows reasonably good agreement with the data, that determined from the previously accepted Born–von Karman parametrization markedly disagrees with experiment. A new parametrization has been found which greatly improves the fit to eigenvector data.

I. INTRODUCTION

The forces between atoms within a crystal are represented by the dynamical matrix, the Fourier transformation of the interatomic force constants. In the harmonic approximation, the eigenvalues of this matrix are the phonon frequencies. As was pointed out by Foreman and Lomer,[1] eigenvector information must also be obtained if the dynamical matrix (and the underlying forces that it represents) is to be determined unambiguously. Recent papers by Leigh, Szigeti, and Tewary[2] and by Cochran[3] point out the inherent difficulties involved in fitting to frequency data alone.

The eigenvectors, however, are not so readily measurable as are the eigenvalues, and certainly far less consideration and effort has gone into their evaluation. The only systematic information obtainable is through the inelastic-neutron-scattering structure factor. This was first pointed out by Brockhouse *et al.*,[4] who went on to measure phonon eigenvectors in this manner in several simple materials. The precautions necessary for obtaining reliable phonon intensities are sufficiently stringent and the measurements themselves sufficiently time consuming that little has been done beyond this initial effort. Identification of eigenvectors of unstable modes involved in structural phase transformations has been attempted in several cases by the Brookhaven group,[5] and Iizumi has recently given a quantitative discussion of phonon intensities in CaF_2.[6] Similar measurements are now in progress on the group-V*A* elements at Los Alamos.[7]

The hexagonal-close-packed (hcp) structure has two atoms per unit cell. Thus this structure is just one step more complicated than those crystals with one atom per unit cell whose structure factors in symmetry directions are completely determined by symmetry considerations alone. A particularly interesting and crucial complication is the lack of inversion symmetry in the hcp structure. This feature makes significant the sign of the phase of the complex dynamical matrix. Of the common hcp metals, Zn was chosen for several reasons. Phonon frequencies have already been determined at many points in the Brillouin zone.[8–12] Attempts to calculate the resulting phonon dispersion relations using pseudopotentials[13,14] are less successful for Zn than for Be or Mg, and in this sense it seems that Zn is less well understood.

The most systematic discussions[9,15] of the lattice dynamics of Zn have been carried out using an entirely phenomenological Born–von Karman-type parametrization of the dynamical matrix of the type suggested by DeWames, Wolfram, and Lehman.[15] Their modified axially symmetric model includes both bond-bending and bond-stretching forces between up to sixth-nearest neighbors, a total of 38 atoms. Forces within the basal plane are independent of direction in that plane. Two parametrizations of this model have been published. The original fit[15] included elastic-constant data as well as the measured frequencies at special points in the Brillouin zone. The second parametrization, due to McDonald, Elcombe and Pryor[9] is a least-squares fit to their measured dispersion curves along three symmetry directions. Since their published parameters give imaginary frequencies in the vicinity of the symmetry point *H*, we have used the original parametrization of this model in all comparisons. A much simpler version of this model is the parametrization of Begbie and Born[16] which includes forces only between the twelve nearest atoms. The structure factors as calculated from this simpler model have been generally used to identify modes in phonon measurements. Contrary to accepted belief, the structure factors calculated from the more complex model differ mark-

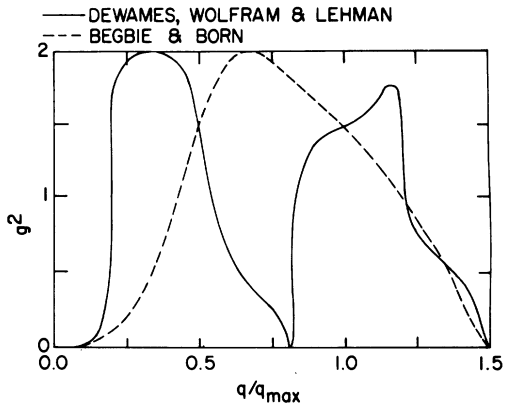

FIG. 1. Inelastic structure factor for the longitudinal optic mode along [010] is shown for two Born–von Karman-type models. The curve due to the simple model of Begbie and Born has generally been used for experimental identification of modes. Contrary to accepted belief, the structure factor predicted by the more complex fit of DeWames *et al.* differs markedly from the earlier values.

edly from the earlier calculation. The most striking difference between models occurs for the longitudinal mode along [010] as is shown in Fig. 1. We have chosen to concentrate on this propagation direction as being possibly the most sensitive to variations between various models.

II. LATTICE DYNAMICS OF AN hcp CRYSTAL

Following the derivation of Maradudin, Montroll, and Weiss,[17] in the harmonic approximation the equation of motion for the displacements $\vec{u}(lk)$ of the kth atom in the lth unit cell of a crystal is given by

$$M_k \ddot{u}_\alpha(lk) = -\sum_{\beta\, l'k'} \Phi_{\alpha\beta}\begin{pmatrix} lk \\ l'k' \end{pmatrix} u_\beta(l'k'), \tag{1}$$

where

$$\Phi_{\alpha\beta}\begin{pmatrix} lk \\ l'k' \end{pmatrix} = \frac{\partial^2 \Phi}{\partial u_\alpha(lk)\, \partial u_\beta(l'k')}\bigg|_{\text{equilibrium}},$$

where α is the direction of displacement, M_k is the mass of the kth atom, while Φ is the potential energy of the crystal. A solution for the displacement associated with the jth mode is of the form

$$u_\alpha(lk) = M_k^{-1/2}\, e_\alpha(k\vec{q}j) \exp[-i\omega_j(\vec{q})t + i\vec{Q}\cdot\vec{R}_l],$$

where $\vec{Q} = \vec{G} + \vec{q}$ is the momentum transferred to the crystal, $\vec{G}$ being a reciprocal-lattice vector. The equations of motion then reduce to

$$\omega_j^2(\vec{q}) e_\alpha(k\vec{q}j) = \sum_{\beta k'} D_{\alpha\beta}(kk' \mid \vec{q})\, e_\beta(k'\vec{q}j), \tag{2}$$

where $D_{\alpha\beta}(kk' \mid \vec{q})$ is the dynamical matrix. For propagation along a high-symmetry direction, the dynamical matrix can often be simplified. For example, if $\vec{q} = (0, \xi, 0)$,

$$D_{\alpha\beta}(kk' \mid \vec{q}) = (M_k M_{k'})^{-1/2} \sum_l \Phi_{\alpha\beta}\begin{pmatrix} lk \\ 0k' \end{pmatrix} e^{i(\vec{q}\cdot\vec{R}_l)}$$

$$= (M_k M_{k'})^{-1/2} \sum_{l_2} F_{\alpha\beta}(kk' \mid l_2)\, e^{2\pi i \xi l_2}, \tag{3}$$

where

$$F_{\alpha\beta}(kk' \mid l_2) = \sum_{l_1 l_3} \Phi_{\alpha\beta}\begin{pmatrix} lk \\ 0k' \end{pmatrix} \tag{4}$$

and

$$\vec{R}_l = (l_1, l_2, l_3).$$

$F_{\alpha\beta}(kk' \mid l_2)$ is, to within a normalizing constant, just the force constant acting between atomic planes perpendicular to $\vec{q}$, separated by l_2 unit cells and on sublattices k and k', respectively. The introduction of interplanar force constants has been used to great advantage in discussing materials with monatomic unit cells.[1,18] However, the method is rather general and we shall see that it is of use in clarifying certain aspects of hcp lattice dynamics as well.

The hcp lattice is composed of two interpenetrating hexagonal sublattices separated by the translation vector $\vec{R}_{12} = (\frac{1}{2}\hat{X}_1 - \frac{1}{3}\hat{X}_2 + \frac{1}{2}\hat{X}_3)$. The vectors $\hat{X}_1$ and $\hat{X}_2$ are Cartesian basis vectors as shown in a projection on the hexagonal basal plane in Fig. 2. $\hat{X}_3$ is the usual basis vector perpendicular to the basal plane. For the [010] propagation direction, it can be shown[19] that the dynamical

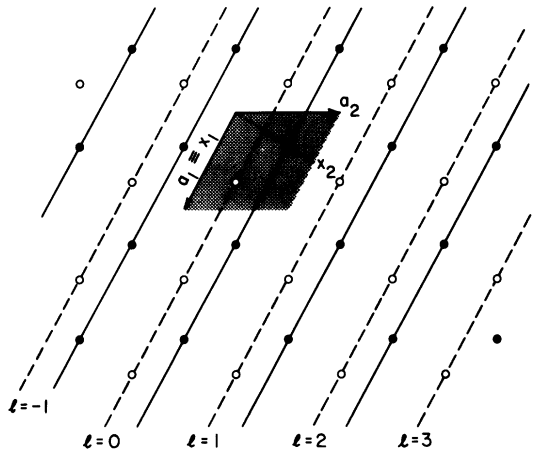

FIG. 2. Basal plane of an hcp crystal showing the planes of atoms which are perpendicular to x_2, the [010] axis. The shaded area indicates the primitive unit cell. Planes are numbered with respect to the plane containing the solid circle within the primitive unit cell. Dashed lines indicate planes belonging to one Bravias sublattice, while solid lines are planes belonging to the other sublattice.

matrix is block diagonalizable. That is, $D_{\alpha\beta}(kk'|\vec{q})$ vanishes unless $\alpha=\beta$. For the [010] longitudinal modes we may then write

$$\omega_{\pm}^2(\vec{q}) = D_{11} \pm |D_{12}|, \tag{5}$$

where

$$D_{yy}(11|\vec{q}) = D_{11},$$
$$D_{yy}(12|\vec{q}) = -|D_{12}|e^{-i\lambda(\vec{q})} = D_{12},$$

where + and − refer to optic and acoustic phonons, respectively. Thus determination of the optic- and acoustic-phonon frequencies yields D_{11} and the magnitude of D_{12} but the phase of D_{12} is unknown. The eigenvector associated with this mode is given by

$$\vec{e}_{\pm}(\vec{q}) = \begin{pmatrix}\vec{e}(1\vec{q}\pm)\\ \vec{e}(2\vec{q}\pm)\end{pmatrix} = \frac{1}{\sqrt{2}}\begin{pmatrix}-1\\ \pm e^{i\lambda(\vec{q})}\end{pmatrix}\hat{e}\ , \tag{6}$$

where $\hat{e}$ is a unit vector along [010]. Thus $\lambda(\vec{q})$ occurring in the dynamical matrix is a very physical quantity. It is just the phase between the motion of the two atomic sublattices.

The one-phonon inelastic neutron scattering is proportional to the inelastic structure factor

$$G_{\pm}^2 = |\vec{Q}\cdot\vec{e}(1\vec{q}\pm) + \vec{Q}\cdot\vec{e}(2\vec{q}\pm)e^{-i\vec{Q}\cdot\vec{R}_{12}}|^2$$
$$= |\vec{Q}\cdot\hat{e}|^2 g_{\pm}^2, \tag{7}$$

where

$$g_{\pm}^2 = 1 \mp \cos(\lambda - \vec{Q}\cdot\vec{R}_{12}).$$

(Structure factors with a different choice of phase factors have appeared in the literature. It is important to make the choice consistent with the choice of phase for the eigenvectors.[7]) Note that $g_+^2 + g_-^2 = 2$, as required by symmetry.[20] Rearranging the above equations we find

$$\cos(\lambda - \vec{Q}\cdot\vec{R}_{12}) = \frac{1-R}{1+R}\ , \tag{8}$$

where $R = g_+^2/g_-^2$, showing that $\lambda(\vec{q})$ is a function only of the *ratio* of the reduced optic and acoustic structure factors. Equation (8) is convenient for deducing $\lambda(\vec{q})$ from experiment, with the single complication that knowing $\vec{Q}\cdot\vec{R}_{12}$, there are still two possible values of $\lambda(\vec{q})$ which satisfy Eq. (8). However, since the dynamical matrix must be real at the zone center and the zone boundary by symmetry,[19] a simple criterion that $\lambda(\vec{q})$ be smooth is adequate to choose a single value of λ over most of the Brillouin zone.

III. EXPERIMENT

The experiments consisted of a series of constant-Q scans of phonon-creation peaks carried out on a triple-axis spectrometer at the Brookhaven High Flux Beam Reactor. Each scan was made versus a fixed monitor count as determined by a monitor placed just before the sample. The initial neutron energy was fixed at 50 meV as determined by a beryllium [110] monochromator. The collimation was 20 min in each position except the analyzer-to-detector position which was 40 min. The detector efficiency was measured to be constant across that range of final neutron energies considered. If the phonon cross section has an energy width negligible compared with the instrumental width and is furthermore essentially constant over that volume in reciprocal space intercepted by the resolution ellipsoid, it can be shown[21] that the peak has a Gaussian energy profile and that the integrated intensity for such a scan is given by

$$I_m = I_0\left(\frac{p_A k_F^3}{\tan\theta_A}\right)\left(\frac{[n_j(\vec{q})+1]e^{-2W}}{\omega_j(\vec{q})}\right)g_j^2|\vec{Q}\cdot\hat{e}|^2 \tag{9}$$

where p_A is the reflectivity of the analyzer crystal, θ_A is the Bragg angle for that crystal, and k_F is the final neutron momentum. $n_j(\vec{q})$ is the Bose-Einstein occupation number $\{\exp[\hbar\omega_j(\vec{q})/k_B T]-1\}^{-1}$ for the jth-phonon mode in a sample at temperature T. W is the Debye-Waller factor and g_j^2 is the reduced inelastic structure factor defined earlier. All remaining factors can be collected into the constant factor I_0.

Data scans were taken at room temperature using a cylindrical sample of $\frac{1}{2}$-in. diameter with mosaic spread of $\sim 0.2°$. The base of the cylinder contained the $[0kl]$ scattering plane in which all our measurements were made. Data were corrected point by point for the reflectivity of the beryllium [002] analyzer, which was measured in a separate experiment. Typical scans are shown in Fig. 3. Except for very small values of q, where the low-energy acoustic phonons were masked by strong Bragg scattering, the energy scans at fixed Q contained both acoustic- and optic-mode peaks. The resulting data were fitted by a nonlinear least-squares procedure to a Gaussian profile with a linearly sloping background. The area of the fitted Gaussian was taken to be the integrated intensity of the peak and corrected for all factors except g_j^2 in Eq. (9). A check against the sum rule which requires optic plus acoustic structure factors to be constant was used to eliminate inconsistent points. A total of three points were discarded in this way.

At the temperature and range of momentum transfer studied here, there is a substantial multiphonon cross section (on the order of 25% of the one-phonon cross section). Within the harmonic approximation, this contributes only to the broad inelastic background which can be dealt with. The potentially more troublesome anharmonic interference between one- and two-phonon terms should

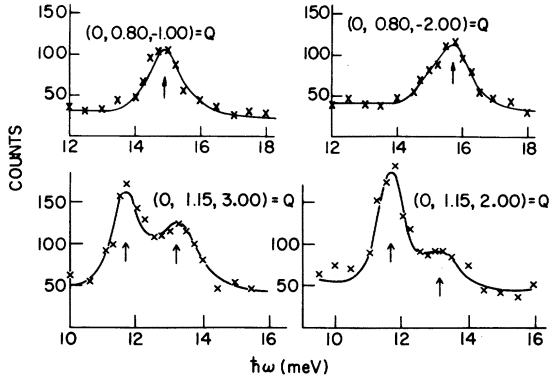

FIG. 3. Typical fits to phonon data for zinc. The solid line is a nonlinear least-squares fit to Gaussian peaks with variable height, width, and center, plus background. Arrows indicate the centers of peaks. The area under each Gaussian is taken to be the integrated intensity of the peak from which structure factors are to be extracted.

manifest itself as a systematic deviation from the sum rule described above. Since we discern no such systematic deviation and since the estimated magnitude of this cross section is less than 10% that of the one-phonon cross section,[22] we have assumed that the intensities measured are due to one-phonon scattering.

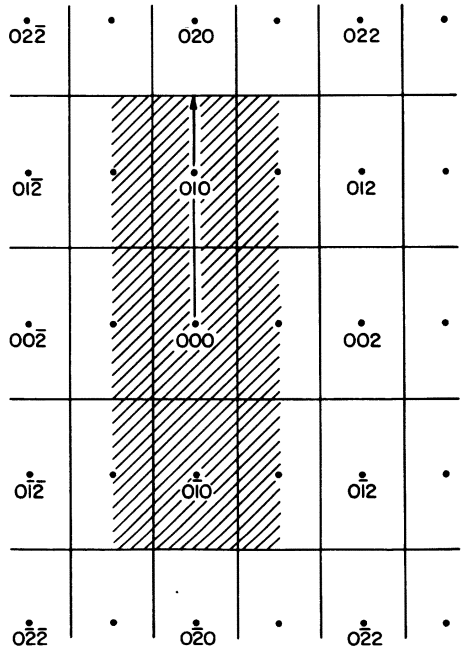

FIG. 4. [0*kl*] plane in reciprocal space showing the zone of the structure factor (shaded area). Arrow indicates the equivalent position in the first-structure-factor zone of the lines covered by the measurements.

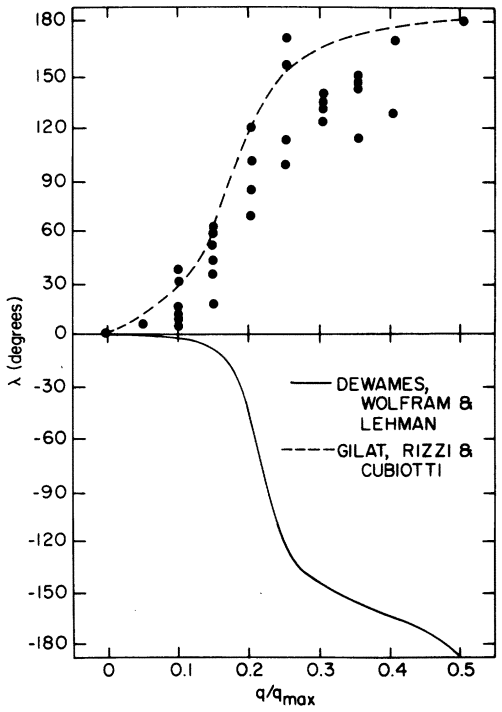

FIG. 5. Measured phase of the motion between atomic sublattices is shown together with two theoretical curves. Points are values extracted from structure-factor measurements. The pseudopotential calculation of Gilat *et al.* is clearly a better description of the data than is the parametrization of DeWames *et al.*

Just as the phonon frequencies and eigenvectors are periodic functions of $\vec{Q}$, so too are the reduced structure factors $g^2_{\pm}(\vec{Q})$ defined in Eq. (7). However the occurrence of the factor $e^{-i\vec{Q}\cdot\vec{R}_{12}}$ causes the repeat distance to be larger than the first Brillouin zone. This larger zone, defined by $g^2(\vec{Q}+\vec{\tau}') = g^2(\vec{Q})$ is known as the zone of the structure factor, and is shown in Fig. 4 for the (0*kl*) plane. There is an additional symmetry relation between the optic and acoustic structure factors which requires that $g^2_{\pm}(0, k, l) = g^2_{\mp}(0, k, l+1)$ for the hcp structure. These redundancies in $g^2_{\pm}(\vec{Q})$ were exploited by measuring $g^2_{\pm}(\vec{Q}+\vec{\tau}')$ for more than one value of $\vec{\tau}'$. The resulting spread in $g^2(\vec{q})$ reduced to the first-structure-factor zone gives a reliable indication of the overall precision of our measurements.

Using Eq. (8) and the measured values of $R = (g_+/g_-)^2$, we obtain the values of $\lambda(\vec{q})$, the phase angles between sublattice oscillations for [010] acoustic modes. These values are indicated by the points in Fig. 5. Although the scatter of points is not small, this arises in part from the nonlinear nature of Eq. (8) which exaggerates the error in λ

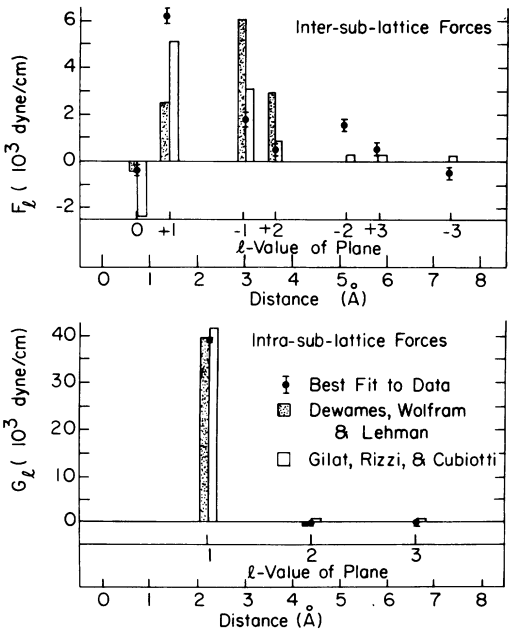

FIG. 6. Magnitude of the interplanar force constants found in the best fit to the combined data for phonon frequencies and $\lambda(q)$. As is expected the nearer planes dominate. Also shown are the force constants obtained from the two theories considered. It should be noted that the constant G_0 is just the sum of all other force constants so that the frequency of the acoustic branch goes to zero at $q=0$. Since G_{-l} is equal to G_l, we have shown values for positive l only. The primary conclusion to be drawn from this set of fits is that discrepancy between models is essentially an interchange of F_1 and F_{-1}.

for a given error in R in some regions of $\vec{Q}$. Shown for comparison in Fig. 5 are the phase angles $\lambda(\vec{q})$ obtained from the eigenvectors of two different model calculations. The first (dotted line) is from the pseudopotential calculation of Gilat, Rizzi, and Cubiotti,[14] which is seen to be in reasonable agreement with the experimentally observed values. The second (solid line) results from the empirical Born–von Karman treatment of DeWames *et al.*[15] The experimental and model phases are seen to disagree as to sign. It should be noted that the sign of $\lambda(\vec{q})$ depends upon the choice of basis vectors. This choice has, however, been made consistently for those quantities compared in Fig. 5. There is thus a real physical difference between the phases represented by the solid and dotted curves in this figure. To see what this difference is and how such a discrepancy might arise, it is useful to discuss now interplanar force constants.

In terms of the interplanar force constants acting between the planes shown in Fig. 2, the longitudinal elements of the dynamical matrix given in Eq. (3) can be written

$$D_{11}(\vec{q}) = G_0 - \sum_{l=1}^{\infty} (G_l + G_{-l}) \cos 2\pi l\xi = \tfrac{1}{2}[\omega_+^2(\vec{q}) + \omega_-^2(\vec{q})],$$

$$D_{12}(\vec{q}) = -F_0 - \sum_{l=1}^{\infty} (F_l + F_{-l}) \cos 2\pi l\xi + i(F_l - F_{-l}) \sin 2\pi l\xi$$

$$= -\tfrac{1}{2}[\omega_+^2(\vec{q}) - \omega_-^2(\vec{q})] (\cos\lambda - i \sin\lambda). \qquad (10)$$

The coefficients $G_l \equiv -M^{-1}F_{yy}(11\,|\,l)$ are the longitudinal force constants between planes separated by $l_2 = l$ unit cells and $F_l \equiv -M^{-1}F_{yy}(12\,|\,l)$ are the corresponding force constants between planes of unlike atoms. G_0 is just the sum of all other force constants to assure $\omega_- = 0$ at $q = 0$. Note that the *intra*sublattice force constants G_l can be derived from frequency measurements alone. The *inter*sublattice forces cannot be determined without additional information which we can take most simply to be the phase information, $\lambda(\vec{q})$. Least-squares fits to Eqs. (10) can be used to determine the interplanar force constants G_l and F_l. The results of such fits are shown in Fig. 6. The values obtained are relatively stable, in the sense that the addition of the $(l+1)$th force-constant parameter has

TABLE I. Interatomic and interplanar force constants for several fits to the model of DeWames *et al.* (Ref. 15) (in units of 10^3 dyn/cm).

Constant	Fit with negative λ	Fit with positive λ	Original fit by DeWames *et al.*
α_1	28.984	29.235	26.650
β_{1x}	−3.370	−3.484	−0.978
β_{1z}	−3.364	−3.347	−3.473
α_4	2.217	2.264	−1.972
β_{4x}	−0.126	−0.104	0.841
β_{4z}	1.029	1.051	0.583
$\alpha_6+\beta_{6z}$	−0.203	−0.075	−1.484
β_{6x}	0.152	0.162	0.624
δ_2	0.556	0.708	0.576
ϵ_{2x}	−0.466	−0.594	−1.027
ϵ_{2z}	−0.441	−2.003	−0.893
δ_3	0.174	0.114	0.158
ϵ_{3x}	−0.960	−0.145	−0.688
ϵ_{3z}	0.129	0.803	−0.241
δ_5	−0.002	−0.009	0.017
ϵ_{5x}	0.471	0.309	0.293
ϵ_{5z}	−0.047	−0.011	0.390
G_0	91.130	91.620	85.750
G_1	37.590	38.310	38.710
G_2	2.090	2.160	−1.130
F_0	2.233	1.652	−0.564
F_1	2.452	5.715	2.330
F_{-1}	5.394	3.999	5.940
F_2	1.688	0.318	2.872

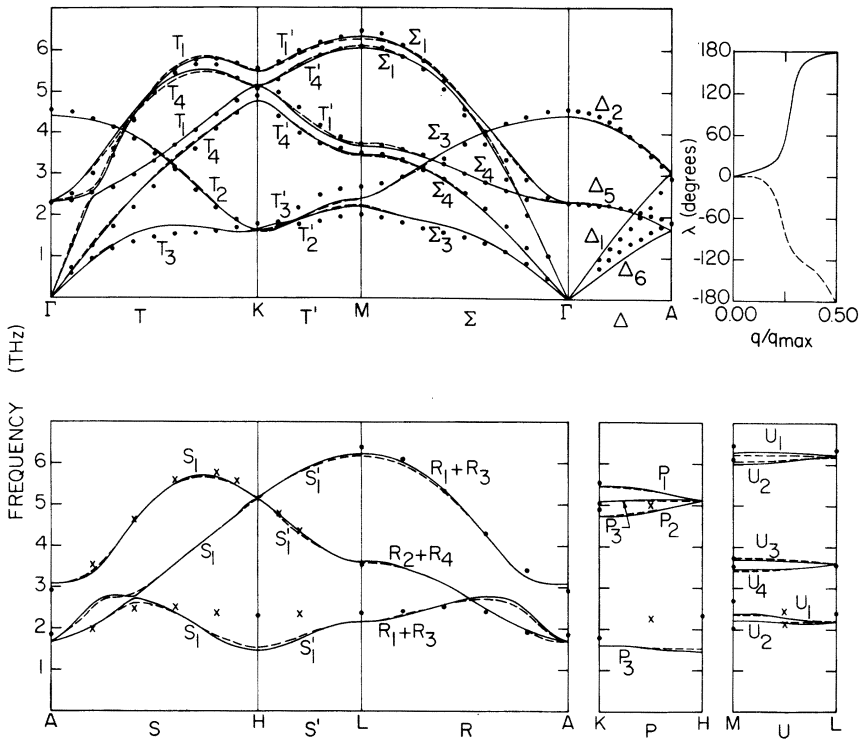

FIG. 7. Comparison of experimental phonon dispersion (Ref. 12) with two fits to the model of DeWames *et al.* The dashed curve is the result of a straight fit to the experimental points marked with a dot. The solid curve is the result of adding a restriction that the phase of λ be positive for the [010] direction. Points marked × were not fit but are shown for completeness. As can be seen, the dispersion curves from the two fits are remarkably similar while λ changes markedly.

little effect on the l parameters previously fit. The fit shown contains 11 intersublattice force constants and 18 intrasublattice force constants. Those not shown in Fig. 6 are zero to within experimental error. The error bars shown reflect the scatter in both frequency and $\lambda(\vec{q})$. Not included however, is an estimate of error due to the finite step size in $\vec{q}$ and the subsequent limit on the number of Fourier coefficients which can be determined. Since it is difficult to estimate the magnitude of this source of error, we feel that these fits should be used primarily in qualitative rather than in quantitative comparisons.

Also shown in Fig. 6 are the interplanar force constants derived from the pseudopotential calculation of Gilat *et al.* and the Born–von Karman model of DeWames *et al.* Note that the intrasublattice coupling is dominated by the near-neighbor term, which is also much greater than any of the intersublattice forces. This feature is correctly reproduced by both models. It is in the intersublattice force constants that the interesting differences arise. Notice, in particular, that both our results and the pseudopotential model suggest that $F_{+1} > F_{-1}$ whereas the parameters selected by DeWames *et al.* result in $F_{-1} > F_{+1}$. It is this interchange of the relative importance of F_{+1} and F_{-1} which is responsible for the very different behaviors of $\lambda(\vec{q})$ shown in Fig. 5. This will be further discussed in the next section.

IV. DISCUSSION

For simplicity let us specialize Eqs. (10) by considering only interplanar force constants up to $l=1$. Writing $\theta = 2\pi\xi$, Eqs. (10) reduce to

$$\tan\lambda = \frac{(F_1 - F_{-1})\sin\theta}{F_0 + (F_1 + F_{-1})\cos\theta} ,$$

$$\omega_+^2 - \omega_-^2 = 2[F_0^2 + F_1^2 + F_{-1}^2 + 2F_0(F_1 + F_{-1})\cos\theta + 2F_1F_{-1}\cos 2\theta]^{1/2} . \qquad (11)$$

Notice that in this approximation an interchange of F_1 and F_{-1} leaves the frequencies unchanged while reversing the sign of λ. More generally, the frequencies in Eqs. (10) are invariant to the complete exchange $F_l \rightarrow F_{-l}$, while this exchange causes $\lambda(\vec{q}) \rightarrow -\lambda(\vec{q})$. Thus we see that phonon-frequency data can be fitted equally well by two solutions which differ by the interchange of F_l and F_{-l}.

The above discussion certainly suggests that a similar ambiguity could be responsible for the apparent reversal of phase of λ which occurs in the model of DeWames *et al.* as shown in Fig. 6. The question now arises as to whether it is possible to adjust the interatomic force constants in such a way as to interchange the interplanar force constants F_l and F_{-l} without adversely affecting the fit to other branches in the dispersion curve. This ad-

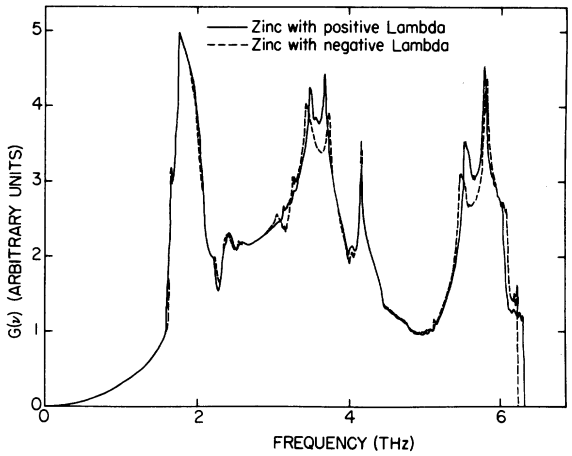

FIG. 8. Frequency distribution functions for the two fits illustrated in the previous figure. As can be seen there is essentially no difference in the frequencies given by the two different sets of interatomic force constants.

justment cannot be made analytically and it was decided to attempt to find a new fit to the model of DeWames *et al.* which would correspond to a positive phase $\lambda(\vec{q})$. We selected the data of Almquist and Stedman[12] as the most complete set of data and performed a least-squares fit to almost all of the available data. (The experimental points shown as × in Fig. 7 correspond to branches in the dispersion curve which could not simply be included in the fitting program.) The resulting interatomic force constants are given in the first column of Table I. The dispersion curves calculated from these parameters are shown as dashed lines in Fig. 7. Also shown is the curve predicted for $\lambda(\vec{q})$. As can be seen, the best fit to the data gives a negative phase as did the original parametrization to this model.

A second fit was then made with the additional constraint that $\lambda(\vec{q})$ be positive at $\vec{q} = 0.5\vec{q}_{max}$. The interatomic force constants obtained under this constraint are given in the second column of Table I. The dispersion curves and phase calculated from these parameters are shown as solid lines in Fig. 7. The dispersion curves obtained are remarkably similar to those obtained from the first fit but the phase is obviously much closer to that obtained in our experiment. The frequency distributions for both fits are shown in Fig. 8. The similarity between these two distributions would seem to indicate that the frequencies away from symmetry directions are essentially the same for both fits. Thus we have generated two sets of interatomic force constants which give nearly identical frequencies throughout the Brillouin zone but which differ markedly in the phase between atomic sublattices.

It should be noted that the calculated standard deviations associated with the interatomic force constants range from 0.1 to 0.4 in both fits. Fluctuations within this range were obtained with variations in fitting procedure. The values shown in Table I represent the best fits as determined by the weighted variance.

Also shown in Table I are the values obtained in the original fit to this model by DeWames *et al.* No apparent pattern in the interatomic force constants occurs upon changing the sign of λ. The interplanar force constants given at the bottom of the table, however, show the expected interchange between F_1 and F_{-1}.

V. CONCLUSION

We have attempted to determine the dynamical matrix elements for longitudinal [010] phonons in zinc by making use of phonon intensities. A best fit to the data gives measured interplanar force constants for planes perpendicular to [010]. A comparison with current models for zinc reveals that the pseudopotential calculation of Gilat, Rizzi, and Cubiotti[14] most closely approximates the data. The original parametrization of the modified axially symmetric model of DeWames, Wolfram, and Lehman[15] predicts a phase between sublattices which is exactly the opposite of that measured in the experiment. Since this model was fitted to only frequency (eigenvalue) data, it is not too surprising that there could be such a large discrepancy since frequency data reveal nothing about this phase. A revised fit to this model was carried out using the most complete frequency data available and restricting the sign of the phase between sublattices. It was found that without this restriction, an equally good fit could be found which differed primarily in the sign of the phase. This alternate fit is a particularly vivid example of the hazards of fitting to eigenvalue data alone which were described by Leigh *et al.*[2] and by Cochran.[3] We believe that this work further demonstrates the desirability of carrying out quantitative phonon-intensity measurements whenever it is practical to do so, particularly in noncentrosymmetric materials.

ACKNOWLEDGMENTS

We would like to thank Dr. R. E. MacFarlane at Los Alamos Laboratory for several helpful discussions on the subtleties involved in intensity measurements. We would also like to thank Dr. G. Gilat for sending us copies of computer printout with numerical values for the dynamical matrix. We are grateful for many beneficial discussions with our colleagues, particularly Dr. G. Shirane and Dr. J. Skalyo, Jr.

*Work performed under the auspices of the U.S. Atomic Energy Commission.

†Work supported by the U.S. Atomic Energy Commission, Grant No. AT(30-1)- 4084 Mod. 1.

‡Present address: Ames Laboratory—U. S. AEC and Department of Physics, Iowa State University, Ames, Iowa 50010.

[1]A. J. E. Foreman and W. M. Lomer, Proc. Phys. Soc. B 70, 1143 (1957).

[2]R. S. Leigh, B. Szigeti, and V. K. Tewary, Proc. R. Soc. A 320, 505 (1971).

[3]W. Cochran, Acta Cryst. A 27, 556 (1971).

[4]B. N. Brockhouse, L. N. Becka, K. R. Rao and A. D. B. Woods, in *Inelastic Scattering of Neutrons in Solids and Liquids* (IAEA, Vienna, 1963), Vol. II, p. 23.

[5]J. Skalyo, Jr., B. C. Frazer, and G. Shirane, Phys. Rev. B 1, 278 (1970); J. D. Axe and G. Shirane, Phys. Rev. B 1, 342 (1970); J. Harada, J. D. Axe and G. Shirane, Acta. Cryst. A 26, 608 (1970).

[6]Masashi Iizumi, J. Phys. Soc. Japan 33, 647 (1972).

[7]R. E. MacFarlane, *The Physics of Semimetals and Narrow Gap Semiconductors*, edited by D. L. Carter and R. T. Bate (Pergamon, New York, 1971); R. E. MacFarlane (private communication).

[8]G. Borgonovi, G. Cagliotti, and J. J. Antal, Phys. Rev. 132, 683 (1963).

[9]D. L. McDonald, M. M. Elcombe, and A. W. Pryor, J. Phys. C. 2, 1857 (1969).

[10]A. J. Millington and G. L. Squires, J. Phys. C 2, 2366 (1969).

[11]G. Cagliotti, G. Rizzi, and G. Cubiotti, Solid State Comm. 8, 367 (1970).

[12]L. Almquist and R. Stedman, J. Phys. F 1, 785 (1971).

[13]E. G. Brovman, Yu Kagan, and A. Holas, in *Inelastic Scattering of Neutrons in Solids and Liquids* (IAEA, Vienna, 1968), Vol. I, p. 165.

[14]G. Gilat, G. Rizzi, and G. Cubiotti, Phys. Rev. 185, 971 (1969).

[15]R. E. DeWames, T. Wolfram, and G. W. Lehman, Phys. Rev. 138, A717 (1965).

[16]G. H. Begbie and M. Born, Proc. R. Soc. Lond. A 188, 179 (1946) and G. H. Begbie, Proc. R. Soc. Lond. A188, 189 (1946).

[17]A. A. Maradudin, E. W. Montroll and G. H. Weiss, in *Solid State Physics*, edited by F. Seitz and D. Turnbull (Academic, New York, 1965), Suppl. 3.

[18]B. N. Brockhouse, T. Arase, G. Caglioti, K. R. Rao, and A. D. B. Woods, Phys. Rev. 128, 1099 (1962).

[19]J. L. Warren, Rev. Mod. Phys. 40, 38 (1968).

[20]R. J. Elliott and M. F. Thorpe, Proc. Phys. Soc. 91, 903 (1967).

[21]N. J. Chesser and J. D. Axe, Acta Cryst. A 29, 160 (1973).

[22]R. A. Cowley, E. C. Svensson, and W. J. L. Buyers, Phys. Rev. Lett. 23, 525 (1969); B. V. Thompson, Phys. Rev. 131, 1420 (1963).